Article

Discovery Medicine 2026; 38(209): 1997–2012
https://doi.org/10.24976/Discov.Med.202638209.155

A New Discovery of Hirudin in Regulating Ferroptosis to Alleviate Ischemic Stroke

Min Shi[1], Fan Sun[2], Yanfei Lu[1], Xiaodong Li[2], Xiaowei Wang[2], Xueyun Liu[2], Xuesong Li[3], Minglei Zhang[4], Wenbing Liu[2,*]

[1]Department of Pharmacy, Zhejiang Rehabilitation Medical Center (The Affiliated Rehabilitation Hospital of Zhejiang Chinese Medical University), 310053 Hangzhou, Zhejiang, China
[2]Department of Cardiopulmonary Rehabilitation, The Third Affiliated Hospital of Zhejiang University of Traditional Chinese Medicine, 310005 Hangzhou, Zhejiang, China
[3]Department of Cardiopulmonary Rehabilitation, Zhejiang Rehabilitation Medical Center (The Affiliated Rehabilitation Hospital of Zhejiang Chinese Medical University), 310053 Hangzhou, Zhejiang, China
[4]Department of Pharmacy, Quzhou Kecheng People's Hospital, 324002 Quzhou, Zhejiang, China
*Correspondence: LIUWENbing_lwb@163.com (Wenbing Liu)
Submitted: 24 September 2025 Revised: 30 April 2026 Accepted: 26 May 2026 Published: 20 June 2026

Background: Ischemic stroke is a major global cause of neurological disability and mortality, triggered by cerebral blood flow occlusion that leads to irreversible brain damage. Ferroptosis, an iron-dependent, lipid peroxidation-driven cell death pathway, contributes significantly to this injury. Hirudin has demonstrated neuroprotective potential in cerebrovascular diseases. This study experimentally validated the molecular mechanism by which hirudin mitigates ischemic stroke through the regulation of ferroptosis, focusing on key signaling pathways and vascular repair.

Methods: *In vivo*, middle cerebral artery occlusion (MCAO) rats were treated with hirudin. Brain injury was evaluated using 2,3,5-Triphenyltetrazolium Chloride (TTC)/terminal deoxynucleotidyl transferase-mediated dUTP nick end labeling (TUNEL) staining. Western blotting was performed to detect ferroptosis (glutathione peroxidase 4 (GPX4) and Solute Carrier Family 7 Member 11 (SLC7A11)) and plasminogen activator, urokinase (PLAU)/nuclear factor kappa-B (NF-κB) proteins. Ferroptosis-related biomarkers (Fe^{2+}, malondialdehyde (MDA), glutathione/glutathione disulfide (GSH/GSSG)) were measured in brain tissues using commercial assay kits. *In vitro*, oxygen-glucose deprivation/reoxygenation (OGD/R)-induced mouse brain endothelial cells (bEnd.3) were treated with hirudin. Cell counting kit-8 (CCK-8) was used to determine optimal hirudin concentration. Lactate dehydrogenase (LDH) release/scratch/tube formation assays were performed to evaluate cell function, while Western blotting and enzyme-linked immunosorbent assay (ELISA) were used to detect related proteins and factors. PLAU-silenced cells were used to verify hirudin's underlying mechanism.

Results: Hirudin reduced MCAO rats' cerebral infarct size and neuronal apoptosis, upregulated GPX4, SLC7A11 and GSH/GSSG, decreased Fe^{2+}, MDA, PLAU, p-65/p65, and inhibited inflammatory factor level ($p < 0.01$). In OGD/R-induced bEnd.3 cells, 1 IU/mL hirudin reduced LDH, promoted cell viability/migration and tube formation, upregulated angiogenesis factors and GPX4/SLC7A11, and downregulated inflammatory factor, PLAU and p-65/p65 levels ($p < 0.01$). Notably, the protective effects achieved by PLAU silencing were comparable to those of hirudin treatment, and their combination did not yield significant additive effects, suggesting that hirudin acts primarily via regulating PLAU.

Conclusion: Hirudin alleviates cerebral ischemic injury and improves ischemic stroke, accompanied by suppression of the PLAU/NF-κB pathway, attenuation of ferroptosis, and enhancement of angiogenesis. These findings clarify hirudin's neuroprotective mechanism and support its potential as a therapeutic agent for ischemic stroke.

Keywords: hirudin; ischemic stroke; angiogenesis; ferroptosis; plasminogen activator, urokinase; nuclear factor kappa-B

Introduction

Stroke refers to cerebrovascular injury or widespread brain tissue injury caused by multiple causes, including ischemic stroke and hemorrhagic stroke, of which ischemic stroke accounts for more than 85% of total stroke cases [1,2]. Ischemic stroke is due to the sudden interruption of cerebral blood flow, resulting in cerebral ischemia, hypoxia, and eventually nerve cell degeneration, apoptosis and neurological dysfunction [3]. Numerous physiological diseases, as well as cellular and molecular mechanisms, including apoptosis, neuroinflammation, oxidative stress, glutamate excitotoxicity, and energy depletion, are involved in the pathological process of ischemic stroke [3,4].

Notably, new angiogenesis plays multiple roles after ischemic stroke. It can restore blood flow to the ischemic boundary area and deliver oxygen and nutrients to damaged brain tissue. Additionally, it stabilizes cerebral perfusion, which promotes axonal growth and neurogenesis. Collectively, these effects improve post-stroke neurological function [5,6]. However, after a stroke, abnormal iron accumulation in the brain triggers ferroptosis, a process closely linked to aggravated tissue damage. Therefore, reducing ferroptosis and lipid peroxidation is of great clinical value for alleviating post-stroke brain injury [7]. Existing studies show a connection between ferroptosis regulation and angiogenesis. For example, upregulating glutathione peroxidase 4 (GPX4) expression to inhibit ferroptosis can enhance angiogenesis in mice with diabetic hindlimb ischemia [8]. Conversely, promoting GPX4-mediated ferroptosis can suppress endothelial cell angiogenesis [9].

Hirudin is the main active component of leech, which can relieve nerve damage and inflammation in acute cerebral stroke [10]. Hirudin also inhibits fibrosis-related angiogenesis [11,12]. In other studies, hirudin inhibits upregulated hypoxia inducible factor-1α (HIF-1α), vascular endothelial growth factor (VEGF), angiopoietin (Ang)-1, and Ang-2 in intracerebral hemorrhage models [13]. In the survival experiment of ischemic flap, hirudin can promote angiogenesis in ischemic flap [14]. Hirudin can also promote the survival of arterialized venous flaps by up-regulating cluster of differentiation 34 (CD34), VEGF, and endothelial nitric oxide synthase (eNOS) [15]. In addition, hirudin can reduce capillary density in the hindlimb ischemia model [16]. At the cellular level, an *in vitro* study has shown that natural hirudin can promote angiogenesis at low doses and inhibit it at high doses [17]. Despite these findings, the specific mechanism by which hirudin regulates angiogenesis and ferroptosis to alleviate ischemic stroke remains unclear.

To address this gap, our previous research first employed network pharmacology to screen potential targets of hirudin in treating cerebral ischemic injury, identifying plasminogen activator, urokinase (PLAU) and nuclear factor kappa-B (NF-κB) as candidate targets. Mechanistically, PLAU can activate the NF-κB pathway [18], and targeting PLAU inhibits NF-κB activation to protect PC12 cells from oxygen-glucose deprivation/reoxygenation (OGD/R)-induced damage [19]. Crucially, NF-κB signaling is involved in the regulation of ferroptosis—its classic pathway (p50/p65 heterodimer nuclear translocation) mediates the transcription of downstream genes, including GPX4 [20,21], while NF-κB inhibition is also associated with angiogenesis in cerebral ischemic injury [22,23].

Based on these findings, we hypothesize that hirudin may alleviate ischemic stroke by downregulating PLAU expression, inhibiting NF-κB p65/p50 nuclear translocation, further promoting downstream GPX4 transcription to suppress ferroptosis, and ultimately enhancing endothelial cell angiogenesis.

Materials and Methods

Animals, Grouping and Middle Cerebral Artery Occlusion (MCAO) Model

The male Sprague-Dawley rats (weighing about 260–280 g, 7–8 weeks old) used in this study were purchased from Hangzhou Medical College. The rats were kept in a pathogen-free environment at 22 $\pm$ 2 °C and subjected to light/dark cycles. Adaptive feeding was continued for one week prior to the experiment. All procedures were approved by the Experimental Animal Welfare Ethics Committee of Zhejiang Experimental Animal Center (NO. ZJCLA-IACUC-20010713). All animal experiments were conducted in accordance with the regulations of the Animal Care and Use Committee.

A total of 18 rats were randomly divided into three groups (n = 6 per group): (1) Sham group: Underwent identical surgical procedures, including anesthesia and vessel exposure, except for the insertion of the occluding filament. (2) Model (Mod) group: Subjected to Middle Cerebral Artery Occlusion (MCAO). (3) Mod+Hirudin (Mod+H) group: Received an intracerebral injection of 10 U hirudin (HY-P2813, MCE, USA) [24].

The MCAO model was established as follows [25]: Rats were anesthetized with 1% pentobarbital sodium solution (P3761, Sigma, Germany), placed on a thermostatically controlled heating pad and kept at 37.0 °C. The right common carotid artery was made visible by the coagulation of the external carotid artery (ECA) distal to the bifurcation. A head-shaped nylon filament was carefully inserted (approximately 18 mm) into the ECA stump to restrict the middle cerebral artery. Following ninety minutes of MCAO, the monofilament was carefully removed to facilitate reperfusion, and the incision was then sutured. The identical treatment was repeated on the rats in the sham group without arterial occlusion. Rats in the MCAO+H group received an intracerebroventricular injection of 10 U hirudin 30 minutes after MCAO induction, and were administered the drug on days 1, 3, and 7 following MCAO. An equal volume of normal saline (ST341, Beyotime, China) was administered to the Mod and Sham groups under the same conditions. On the second day of the last administration, the rats were deeply anesthetized with 1% sodium pentobarbital solution. After collection of the required tissues, all animals were euthanized by an overdose of the same anesthetic (160 mg/kg, intraperitoneally), followed by confirmation of cardiac arrest. This euthanasia procedure complies with the AVMA Guidelines and was approved by the ethics committee. Brain tissues were then dissected for subsequent analyses.

2,3,5-Triphenyltetrazolium Chloride (TTC) Staining

The brain samples were frozen at –20 °C for twenty minutes and were then sectioned into approximately 2 mm-thick slices. Following the instructions of the TTC

kit (60508ES25, Yeasen, China), staining was performed at 37 °C. After staining, the brain slices were fixed in 4% paraformaldehyde solution (A501912-0500, Sangon Biotech, China) for 24 hours (h). Infarct size was quantitatively assessed using ImageJ software (version 1.8.0, National Institutes of Health (NIH), Bethesda, Maryland, USA).

Evans Blue Assay

To assess blood-brain barrier integrity, Evans Blue dye (E2129, Sigma-Aldrich, USA) was administered intravenously via the tail vein on day 7 after MCAO surgery. Each rat received 4 mg of Evans Blue dissolved in 200 µL of sterile normal saline. After allowing 24 h for dye circulation and extravasation, rats were deeply anesthetized and subjected to transcardial perfusion with 20 mL of ice-cold saline to remove intravascular dye. The brains were then harvested and sectioned coronally into 1-mm-thick slices using a rodent brain matrix. Macroscopic images of the brain slices were captured under consistent lighting to document Evans Blue leakage.

Terminal Deoxynucleotidyl Transferase-Mediated dUTP Nick End Labeling (TUNEL) Staining

Gradient ethanol (C06915101, Nanjing Reagent, Nanjing, China) and xylene (C04305302, Nanjing Reagent, Nanjing, China) were used to dewax paraffin slices of the produced brain tissue. Apoptosis for paraffin-embedded tissues was detected using a One Step TUNEL Apoptosis Assay Kit (C1091, Beyotime, Shanghai, China) according to the manufacturer's protocol. Briefly, after antigen retrieval with Proteinase K (20 µg/mL) at 37 °C for 20 min, endogenous peroxidases were inactivated by incubation with 3% H_2O_2 for 20 min at room temperature. Sections were then incubated with the TUNEL reaction mixture containing TdT enzyme and biotin-dUTP at 37 °C for 60 min in a humidified dark chamber. After stopping the reaction, sections were incubated with Streptavidin-HRP working solution for 30 min at room temperature. Sections were developed using a 3,3'-diaminobenzidine (DAB) chromogen substrate kit until appropriate staining intensity was achieved (10 min). Finally, sections were counterstained with hematoxylin, dehydrated, cleared, and mounted. TUNEL-positive cells (brown nuclei) and total cells (blue nuclei) were observed and counted under a light microscope (NIB900-FL, Nexcope, China) at 100× magnification. The apoptotic index was calculated as the percentage of TUNEL-positive cells.

Immunofluorescence

Fresh brain tissue was fixed in 4% paraformaldehyde for 12 h, and then rinsed three times with phosphate-buffered saline (PBS, AC13319, Acmec, Shanghai, China). 0.3% Triton-X100 (X100, Sigma-Aldrich, St. Louis, MO, USA) was added, followed by incubation for 30 min at room temperature, and the samples were then rinsed with PBS (ST477, Beyotime, Shanghai, China). We added 3% bovine serum albumin (10711454001, Roche, Basel, Switzerland) and incubated the samples at room temperature for 2 h. The specific primary antibody CD31 (sc-18916, 1: 200, Santa Cruz Biotechnology, Dallas, TX, USA) was applied, followed by sealing with a coverslip and incubation in a humidified chamber at 4 °C overnight. Following three PBS washes, the secondary antibody (A-11007, Thermo Fisher Scientific, Waltham, MA, USA) was added and incubated for 2 h. PBS-diluted 4',6-Diamidino-2'-phenylindole (DAPI) staining solution (C1005, Beyotime, Shanghai, China) was added. After being stained for 5 min at room temperature, the sample was examined using a fluorescent microscope (NIB900-FL, Nexcope, Ningbo, China).

Cell Culture, Modeling, and Grouping

Mouse brain endothelial cells bEnd.3 were purchased from American Type Culture Collection (Manassas, VA, USA) [26]. Cells were cultured under standard conditions and their morphology was routinely monitored under a phase-contrast microscope to confirm typical endothelial cobblestone appearance, consistent with bEnd.3 cell characteristics. The test result for mycoplasma contamination of cells was negative.

Cell counting kit-8 (CCK-8) was used to screen the optimal dose of hirudin (0.5 IU/mL, 1 IU/mL, 5 IU/mL) to promote the activity of mouse bEnd.3 cells. Based on a preliminary CCK-8 assay that identified 1 IU/mL as the optimal dose, subsequent experiments were conducted with three groups: a Con group, a Mod-oxygen-glucose deprivation/reoxygenation (OGD/R) group, and a Mod+H group (1 IU/mL hirudin was added for intervention according to the results of the CCK-8 experiment after modeling).

To establish an *in vitro* ischemia-reperfusion model [27], the cells were subjected to oxygen and glucose deprivation (OGD), and the cells were cultured at 1% O_2, 5% CO_2, 94% N_2, and 37 °C for 6 h. After 6 h of OGD exposure, the cells were rinsed and incubated under normal conditions, a reoxidation process. OGD/R was used to induce cellular injury.

PLAU Silencing and Experimental Grouping

Then the cells were divided into 5 groups: a Con+shRNA negative control (shNC) group (transfected shNC), a Mod+shNC group (transfected shNC and treated with OGD/R), a Mod+shRNA PLAU (shPLAU) group (transfected shPLAU and treated with OGD/R), a Mod+H+shNC group (transfected shNC and treated with OGD/R and hirudin intervention), and a Mod+H+shPLAU group (transfected shPLAU and treated with OGD/R and hirudin intervention).

The shPLAU (pLV[shRNA]-EGFP/Puro-U6>mPlau[shRNA#1], 5′-

GCUCAAGGCUUAACUCCAATT-3′) and shNC (5′-GCTTCGCGCCGTAGTCTTA-3′) were purchased from Yunzhou Biosciences Co., Ltd. (Guangzhou, China). The transfection efficiency was detected 48 h after sh-PLAU transfection using quantitative reverse transcription polymerase chain reaction (qRT-PCR).

CCK-8 Assay

5×10^3 cells were added to each well of the 96-well plates for inoculation. As per the experimental protocol, distinct cell groups were treated and cultured at 37 °C and 5% CO_2 for 48 h, respectively. Following the culture procedure, 10 µL of CCK-8 solution (HY-K0301, MCE, Monmouth Junction, NJ, USA) was applied to each well, and then incubated for 2 h at 37 °C in an incubator (Forma Steri-Cult, Thermo Fisher Scientific, Waltham, MA, USA). Using an enzyme labeler, cell viability was calculated, and the absorbance at 450 nm was observed. Relative cell viability (%) = $(OD_{experiment} - OD_{blank}) / (OD_{control} - OD_{blank}) \times 100\%$. Values were then normalized against the Control group.

LDH Level Detection

The appropriate number of cells was inoculated onto the 96-well plates based on cell size and growth rate, ensuring that the tested cell density did not exceed 80–90%. Cells were then treated with the drugs. Following medication stimulation, the plates were centrifuged at 400 rpm for 5 min using a perforated plate centrifuge. As directed by the LDH kit (C0016, Beyotime, Shanghai, China), the LDH levels were measured by assessing the absorbance of each well at 490 nm using an enzyme-labeled equipment.

Cell Scratch Test

Cells were inoculated into 6-well plates at 1×10^5 cells/well and cultured until 90% confluent. According to the specific requirements of the experiment, cells were subjected to the modeling or PLAU silence followed by drug treatment. The cells were scratched straight using a pipette tip and cleaned twice with PBS. Images were captured using a optical microscope (THUNDER Imager Tissue, Leica, Wetzlar, Germany) at 0 h and 24 h after scratching. The cells were in serum starvation state during the assay. Relative migration rate (%) = (0 h scratch width – 24 h scratch width) / 0 h scratch width × 100%.

Tube Forming Experiment

The pipette tips and 96-well plates were pre-cooled in the refrigerator for 1 h before the experiment. Subsequently, 50 µL pre-thawed Matrigel (354230, Corning, USA) was added to each well of the 96-well plate and incubated at 37 °C for 30 minutes to allow solidification. The cells were digested and resuspended in the medium of each group, and 100 µL of cell suspension (1.0×10^4 cells/mL) was seeded into each well. The cells were then cultured in a 5% CO_2 incubator at 37 °C for 4–6 h, and imaged under a microscope (THUNDER Imager Tissue, Leica, Wetzlar, Germany).

qRT-PCR

With the use of the Eastep Super Total RNA extraction kit (ls1040, Promega, Madison, WI, USA), total RNA was extracted from cells or tissues. Single-strand complementary DNA (cDNA) was synthesized by reverse transcription using a cDNA reverse transcription mix (R323-01, Vazyme Biotech, Nanjing, China). qPCR was performed using a qRT-PCR system (ABI7500, Applied Biosystems) with target gene-specific primers (Table 1) and GAPDH as an internal reference. The relative gene expression was calculated with the $2^{-\Delta\Delta Ct}$ method [28].

Enzyme-Linked Immunosorbent Assay (ELISA)

The rat inflammatory cytokines interleukin (IL)-1β (88-6010A-22, Thermo Fisher Scientific, Waltham, MA, USA), rat IL-6 (BMS625, Thermo Fisher Scientific, USA) and rat tumor necrosis factor-α (TNF-α, KRC3011, Thermo Fisher Scientific, USA) in brain tissue, or mouse vascular endothelial growth factor A (VEGF-A) ELISA Kit (BMS619-2TEN, Thermo Fisher Scientific, USA), mouse brain-derived neurotrophic factor (BDNF) ELISA Kit (EEL088, Thermo Fisher Scientific, USA), mouse basic fibroblast growth factor (bFGF) ELISA Kit (EMFGF2, Thermo Fisher Scientific, USA), mouse angiostatin ELISA Kit (abx153635, Abbexa, Cambridge, UK) and mouse endostatin ELISA Kit (EM25RB, Thermo Fisher Scientific, USA) in bEnd.3 cells were detected with ELISA kit. Following each kit's instructions, factor concentrations were calculated accordingly. 100 µL primary antibody was added to each well of a white microplate, and incubated at 37 °C for 4 h. Then, the solution was discarded, and blocking buffer was added, followed by incubation at 37 °C for 1 h. Subsequently, the wells were washed 3 times with washing buffer. After removing residual liquid, 100 µL cell supernatant was added and incubated at 37 °C for 1 h, followed by 3 washes. Substrate solution was added, and after incubation at 37 °C for 1 h with enzyme-labeled antibody, the reaction was terminated using stop solution. Absorbance was measured using an ELISA microplate reader at 450 nm or 550 nm.

Western Blotting

Total proteins were extracted from rat brain tissue or bEnd.3 cells using radioimmunoprecipitation assay (RIPA) lysis buffer (R0010, Solarbio, China) containing protease and phosphatase inhibitors, and the bicinchoninic acid (BCA) method was used to assess the protein concentration. Proteins were separated via electrophoresis on sodium dodecyl sulfate-polyacrylamide gel electrophoresis (SDS-PAGE, P0012A, Beyotime, China) gels and then transferred onto polyvinylidene fluoride (PVDF) membrane (YA1700,

Table 1. Primer sequences utilized in the qRT-PCR experiment.

Target Gene	Forward Primer (5′-3′)	Reverse Primer (5′-3′)	Species
GAPDH	GCCAGCCTCGTCTCATAGACA	GTCCGATACGGCCAAATCC	Rat
IL-1β	TCAGGAAGGCAGTGTCACTCATTG	ACACACTAGCAGGTCGTCATCATC	
IL-6	CTAGTGCGTTATGCCTAAG	CCATCTGGCTAGGTAACA	
TNF-α	TGAACTTCGGGGTGATCG	GGGCTTGTCACTCGAGTTTT	
GAPDH	GAGGACCAGGTTGTCTCC	CCTTGGAGGCCATGTAGG	Mouse
IL-1β	GTGGCTGTGGAGAAGCTGTG	GAAGGTCCACGGGAAAGACAC	
IL-6	CCAGAAACCGCTATGAAGTTCC	TTGTCACCAGCATCAGTCCC	
TNF-α	ACAGAAAGCATGATCCGCG	GCCCCCCATCTTTTGGG	

GAPDH, glyceraldehyde-3-phosphate dehydrogenase; IL, interleukin; TNF-α, tumor necrosis factor-α.

Solarbio, China). The membrane was blocked with 5% skim milk at room temperature for 1.5 h, followed by overnight incubation at 4 °C with the following primary antibodies: GPX4 (ab125066, Abcam, UK, 17 kDa, 1:1000), Solute Carrier Family 7 Member 11 (SLC7A11, ab307601, Abcam, UK, 50 kDa, 1:1000), PLAU (17968-1-AP, Proteintech, Wuhan, China, 49 kDa), p-p65 (ab76302, Abcam, UK, 65 kDa, 1:1000), p65 (ab19870, Abcam, UK, 64 kDa, 1:1000), vascular endothelial growth factor A (VEGFA, ab214424, Abcam, UK, 23 kDa,1:500), Vascular endothelial growth factor receptor-2 (VEGFR2, ab221679, Abcam, UK, 180 kDa, 1:1000), glyceraldehyde-3-phosphate dehydrogenase (GAPDH, ab181602, Abcam, UK, 37 kDa, 1:500). After washing, the membranes were incubated with the corresponding secondary antibody Goat Anti-Rabbit IgG H&L (HRP) (ab6721, Abcam, UK, 1:2000) for 2 h at room temperature. The gel imaging system was used to visualize the bands, and ImageJ software (version 1.8.0, National Institutes of Health (NIH), Bethesda, Maryland, USA) was used to analyze the gray values.

Malondialdehyde (MDA), Glutathione/Glutathione Disulfide (GSH/GSSG) and Iron Assay

The tissues or cells were weighed and homogenized in a suitable volume of pre-chilled physiological saline (ST341, Beyotime, China). The homogenate was then centrifuged at 3000 rpm for 10 min at 4 °C to obtain the supernatant. Subsequently, following the instructions of the respective commercial kits for MDA (S0131S, Beyotime, China), reduced GSH/GSSG (S0053, Beyotime, China), and ferrous ion (Fe^{2+}, MAK025, Merck, Germany), appropriate volumes of the supernatant were taken to perform the detection reactions. The absorbance values of the reaction solutions were measured using a microplate reader (Varioskan LUX, Thermo Fisher, USA) at the designated wavelengths (450/412/593 nm), and the concentrations of MDA, GSH/GSSG, and Fe^{2+} in the brain tissues were calculated based on the standard curves provided by the kits.

Statistical Analysis

Statistical analysis was performed using GraphPad Prism 8.0 (GraphPad Software, Inc, San Diego, CA, USA). Measurement data are expressed as Mean $\pm$ standard (SD). The data were tested for normality using the Shapiro-Wilk test, and homogeneity of variances was evaluated using Levene's test. One-way analysis of variance (ANOVA) followed by Tukey post hoc test was employed to compare data across multiple groups. A $p < 0.05$ was regarded as statistically significant.

Results

Analysis of TTC Evans Blue and TUNEL Staining Results

We conducted TTC staining test to detect the improvement effect of hirudin on the cerebral ischemic area in MCAO rats. Compared to the sham operation group, the cerebral infarction area in the model group was considerably greater, indicating successful modeling ($p < 0.001$, Fig. 1A,B). After hirudin treatment, the cerebral infarction size in rats was notably lower than that in the model group ($p < 0.001$, Fig. 1A,B). This suggests that hirudin can reduce ischemic brain area in the MCAO rats. In addition, Evans blue assay results showed that Evans blue accumulation was increased in the injured cortex after MCAO, while Evans blue accumulation was decreased after hirudin treatment ($p < 0.001$, Fig. 1C,D). TUNEL staining was performed in different groups, and apoptotic cell nuclei were stained brown, showing positive results. Cellular apoptosis was significantly intensified after modeling, as shown in Fig. 1E,F ($p < 0.001$). After hirudin treatment, apoptosis was improved and TUNEL-positive expression decreased (Fig. 1E,F, $p < 0.001$).

Immunofluorescence Staining and Angiogenis-Related Protein Expression in Brain Tissues

In order to explore the effects of hirudin on angiogenesis, we detected the CD31 protein mainly expressed in vascular endothelial cells in brain tissue (Fig. 2A,B). As shown in Fig. 2A,B, the nucleus exhibited blue fluorescence and the CD31 protein expression was indicated by red fluorescence. Compared to the sham group, the CD31 positive area in the model group was lower, but after hirudin interven-

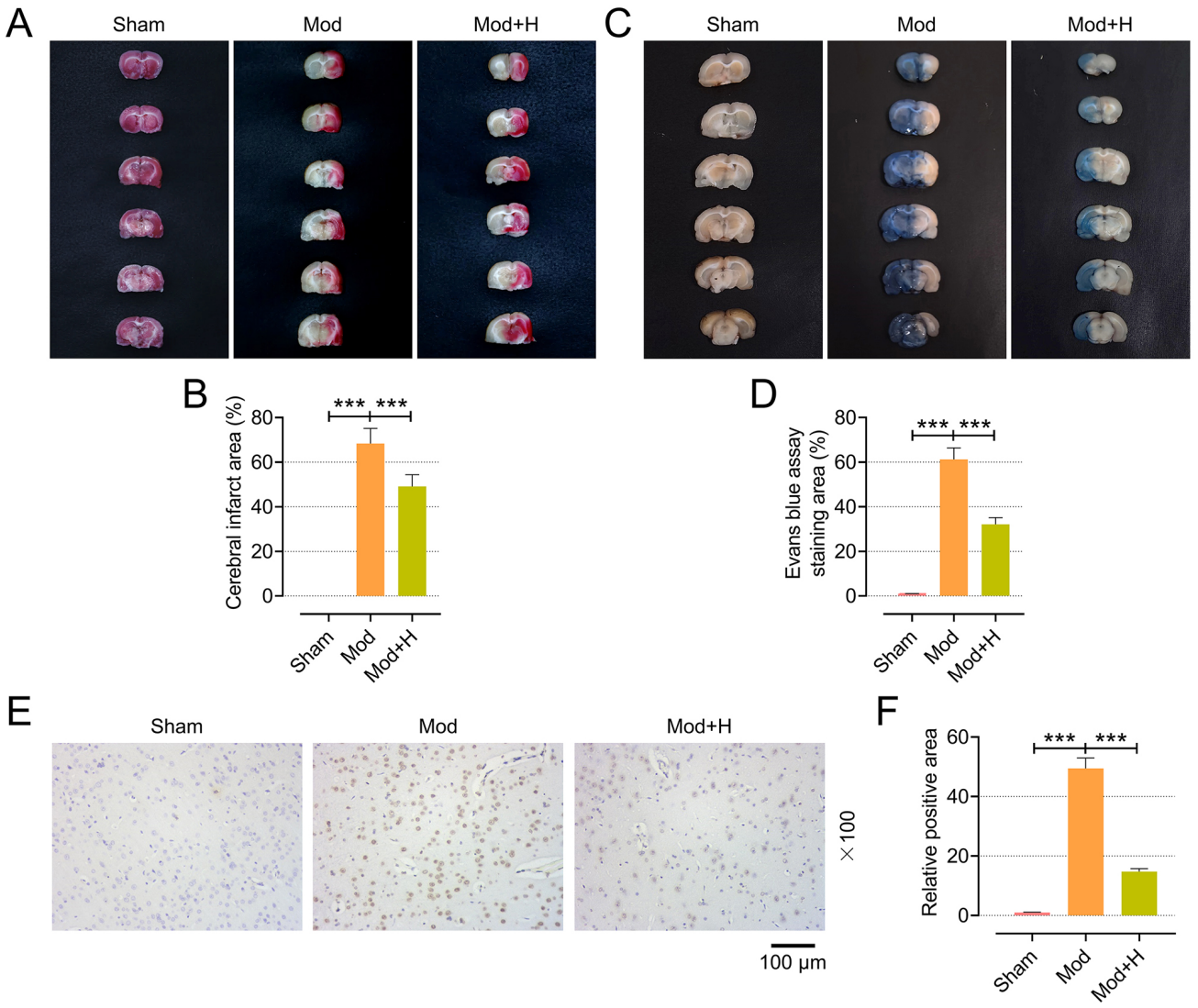

Fig. 1. Hirudin reduces the area of brain ischemia, protects the blood-brain barrier integrity and inhibits cell apoptosis. (A,B) The infarct size was measured using 2,3,5-Triphenyltetrazolium chloride (TTC) staining. (C,D) The blood-brain barrier integrity was assessed using Evans blue staining. (E,F) Apoptosis was observed using Terminal Deoxynucleotidyl Transferase-Mediated dUTP Nick End Labeling (TUNEL) staining in brain tissue (scale bar: 100 μm, magnification; ×100). Each group consisted of 6 rats. ***$p < 0.001$.

tion, the CD31 positive area was enhanced ($p < 0.01$). In the detection of angiogenis-related proteins, we found that the expression levels of VEGFA and VEGFR2 proteins decreased after modeling compared with the sham group ($p < 0.001$, Fig. 2C,D). Hirudin treatment could increase the expression of these two proteins in MCAO rats, which was significantly higher than that in the model group ($p < 0.01$, Fig. 2C,D). These findings show that hirudin can promote angiogenesis in MCAO rats.

Detection of Protein Expression, Inflammatory Factor Levels, MDA, GSH/GSSG and Iron in Brain Tissue

In our study, the Western blotting was used to determine the expression of PLAU/NF-κB and ferroptosis-related proteins in brain tissues. qRT-PCR and ELISA were used to determine the amounts of inflammatory factors in brain tissues. The levels of MDA, GSH/GSSG and Fe^{2+} were detected using the corresponding assay kit. After modeling, in comparison to the sham group, rats in the model group exhibited considerably higher levels of IL-1β, IL-6, and TNF-α in brain tissues ($p < 0.001$, Fig. 3A–F), indicating that inflammation occurred in the brain tissue and inflammatory factors were secreted. Hirudin treatment reversed the expression trend of inflammatory factors after modeling; IL-1β, IL-6 and TNF-α levels were inhibited compared with the MCAO rats ($p < 0.01$, Fig. 3A–F). In the ferroptosis protein detection, hirudin treatment could reverse the downregulated levels of GPX4 and SLLC7A11 proteins after the model establishment ($p < 0.01$, Fig. 3G–I). Furthermore, compared with the sham group, the levels of MDA and Fe^{2+} in MCAO rats increased, while the level

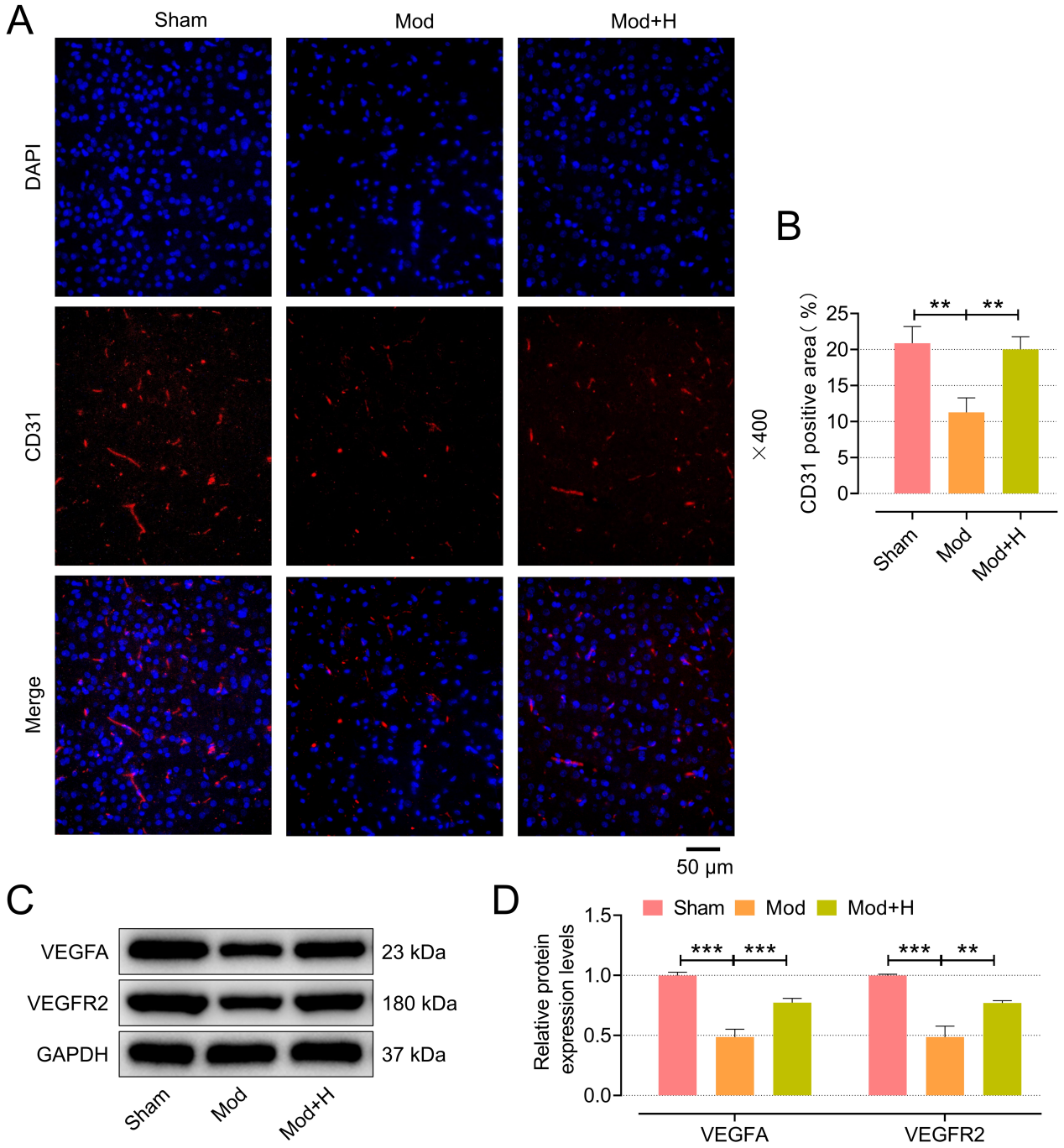

Fig. 2. Hirudin promotes angiogenesis in brain tissue. (A,B) The expression of platelet endothelial cell adhesion molecule-1 (CD31) in brain tissue was detected by immunofluorescence (scale bar: 50 μm, magnification; ×400). (C,D) The expression of vascular endothelial growth factor A (VEGFA) and vascular endothelial growth factor receptor-2 (VEGFR2) in brain tissue was detected by Western blotting. Glyceraldehyde-3-phosphate dehydrogenase (GAPDH) was the internal parameter. Each group consisted of 6 rats. $^{**}p < 0.01$, $^{***}p < 0.001$.

of GSH/GSSG decreased ($p < 0.001$, Fig. 3J–L). Hirudin treatment alleviated these changes in MDA, GSH/GSSG and Fe^{2+} levels ($p < 0.001$, Fig. 3J–L). These results reveal that Hirudin inhibited the ferroptosis process during the treatment of ischemic stroke. The results of PLAU/NF-κB expression detection confirmed that hirudin could inhibit the expression of PLAU/NF-κB. After modeling, PLAU and p-p65/p65 levels in brain tissue increased significantly compared with those of the unmodeled rat ($p < 0.001$, Fig. 3M–O). In the brain tissue of MCAO rats, hirudin therapy could reduce the expression of PLAU and p-p65/p65 levels; this difference was noteworthy when compared to rats in the model group ($p < 0.001$, Fig. 3M–O).

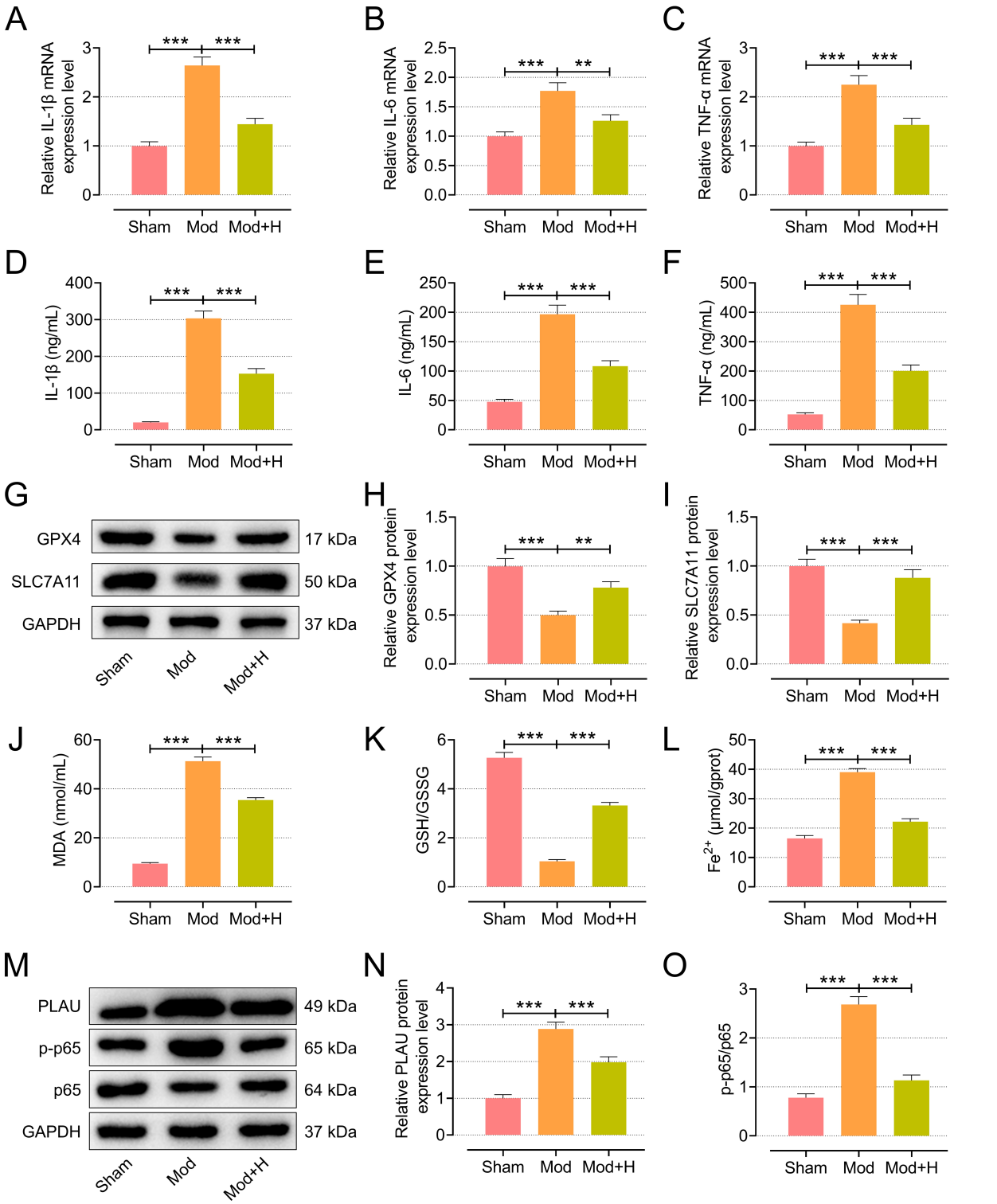

Fig. 3. Hirudin inhibits inflammation, ferroptosis indicators, as well as plasminogen activator, urokinase (PLAU)/nuclear factor kappa-B (NF-κB). (A–C) The expression of inflammatory cytokines interleukin (IL)-1β, IL-6 and tumor necrosis factor-α (TNF-α) in brain tissue was detected by quantitative reverse transcription polymerase chain reaction (qRT-PCR). (D–F) Enzyme-Linked immunosorbent Assay (ELISA) detects levels of the inflammatory factors IL-1β, IL-6 and TNF-α in brain tissue. (G–I) The expression of glutathione peroxidase 4 (GPX4) and solute carrier family 7 member 11 (SLC7A11) in brain tissue was detected by Western blotting. GAPDH was used as the internal reference. (J–L) The levels of malondialdehyde (MDA), glutathione (GSH)/glutathione disulfide (GSSG) and Fe^{2+} were detected by the corresponding assay kit. (M–O) The expression of PLAU/NF-κB in brain tissue was detected by Western blotting. GAPDH was used as the internal reference. Each group consisted of 6 rats. $^{**}p < 0.01$, $^{***}p < 0.001$.

Cell Viability, LDH Levels, Migration and Angiogenesis Were Measured

Firstly, different concentrations of hirudin (0.5 IU/mL, 1 IU/mL, 5 IU/mL) were used to interfere with the growth activity of bEnd.3 cells after OGD/R, and the optimal concentration to promote bEnd.3 cells growth activity was screened. As depicted in Fig. 4A, the moderate dose of hirudin most effectively promoted bEnd.3 cells activity, with a significant difference compared with the model group ($p < 0.05$, Fig. 4A). Therefore, we chose 1 IU/mL hirudin for follow-up experiments. Following cell modeling and drug administration, the LDH level was measured. The LDH level of the model group was much higher than that of the control group, and the hirudin intervention resulted in a significant decline in LDH level relative to the model group ($p < 0.01$, Fig. 4B). After modeling, the cell migration rate in the model group was lower than that in the control group, while hirudin intervention promoted the migration ($p < 0.001$, Fig. 4C,D). We also conducted tube formation experiments to explore hirudin's ability to promote cell tube formation. The results show that the cell tube length in the model group was smaller than that in the control group, and hirudin intervention significantly increased the cell tube length after modeling, as shown in Fig. 4E,F ($p < 0.001$).

Cell Protein, Inflammatory Factor, MDA, GSH/GSSG and Iron Assay Results

We detected the expression of VEGFA and VEGFR2 by Western blotting. Compared with the control group, the expression of VEGFA and VEGFR2 in bEnd.3 cells in the model group was down-regulated, which was reversed by hirudin treatment, and the expression levels of these two proteins were significantly up-regulated compared with the model group ($p < 0.001$, Fig. 5A–C). The Mod-OGD/R group had increased expression levels of inflammatory cytokines, such as IL-1β, IL-6, and TNF-α, compared to the control group, according to the results of qRT-PCR ($p < 0.001$, Fig. 5D–F). In modeled cells, hirudin intervention could significantly reduce the expression of TNF-α, IL-6, and IL-1β when compared to the model group ($p < 0.01$, Fig. 5D–F). Furthermore, hirudin treatment could reverse the downregulation of GPX4, SLC7A11, and GSH/GSSG caused by OGD/R modeling, as well as the promotive effect on MDA and Fe^{2+} ($p < 0.05$, Fig. 5G–L). Lastly, Western blotting was used to determine the PLAU and p-p65/p65 protein expression levels in each group. Compared with the control group, the levels of PLAU and p-p65/p65 were significantly up-regulated after modeling, and the related proteins in the Mod+H group were significantly down-regulated compared with the model group ($p < 0.001$, Fig. 5M–O).

Effects of Hirudin and PLAU Silencing on PLAU/NF-κB Expression, Cell Viability and Migration Ability in bEnd.3 Cells

After PLAU silencing, the transfection efficiency was detected by qRT-PCR. Results as shown in Fig. 6A, compared with the shNC group, PLAU mRNA expression in bEnd.3 cells decreased after PLAU silencing, indicating successful transfection ($p < 0.001$). The protein levels of PLAU and p-p65/p65 in each group were measured by Western blotting. Compared with the Con+shNC group, PLAU and p-p65/p65 protein levels were shown to be substantially increased in Mod+shNC group ($p < 0.001$, Fig. 6B–D). After transfection with shPLAU or transfection with shNC and intervention with hirudin, the expressions of PLAU and p-p65/p65 in cells were lower than those in the Mod+shNC group ($p < 0.001$, Fig. 6B–D). CCK-8 detected the cell viability of different groups, and the results are shown in Fig. 6E. The cell viability of the Mod+shNC group was lower than that of the Con+shNC group, and the cell viability of the Mod+shPLAU and Mod+H+shNC groups was significantly increased compared with the Mod+shNC group ($p < 0.01$, Fig. 6E). We then performed cell scratch experiments and found that cell migration rate in the Mod+shNC group was lower than that in the Con+shNC group at 24 h, while cell migration rate in the Mod+shPLAU and Mod+H+shNC groups was significantly higher than that in the Mod+shNC group ($p < 0.001$, Fig. 6F,G).

Effect of Hirudin and PLAU Silencing on Expression of Angiogenic, Angiogenic Factor and Ferroptosis in bEnd.3 Cells

We examined the expression of angiogenic protein in the cells of each experimental group. Results as shown in Fig. 7A–C, compared with the Con+shNC group, the protein levels of VEGFA and VEGFR2 in the Mod+shNC group were significantly decreased, while the expression levels of VEGFA and VEGFR2 in the Mod+shPLAU and Mod+H+shNC groups were higher than those in the Mod+shNC group ($p < 0.05$). Then, we used ELISA to detect the secretion of VEGF, BDNF, bFGF, angiostatin and endostatin. The test results are shown in Fig. 7D–H. The secretion of angiogenic-related factors in the Mod+shNC group was lower than that in the Con+shNC group ($p < 0.001$). The levels of angiogenic-related factors in the Mod+shPLAU and Mod+H+shNC groups were significantly up-regulated compared with those in the Mod+shNC group ($p < 0.05$). The levels of VEGF, bFGF and endostatin in the Mod+H+shPLAU group were higher than those in the Mod+H+shNC group ($p < 0.05$). Finally, we found that in the Mod+shNC group, GPX4, SLC7A11 and GSH/GSSG were downregulated, while MDA and Fe^{2+} levels were upregulated compared with the Con+shNC group ($p < 0.01$, Fig. 7I–N). In contrast, hirudin treatment or PLAU knockdown reversed this regulatory process (p

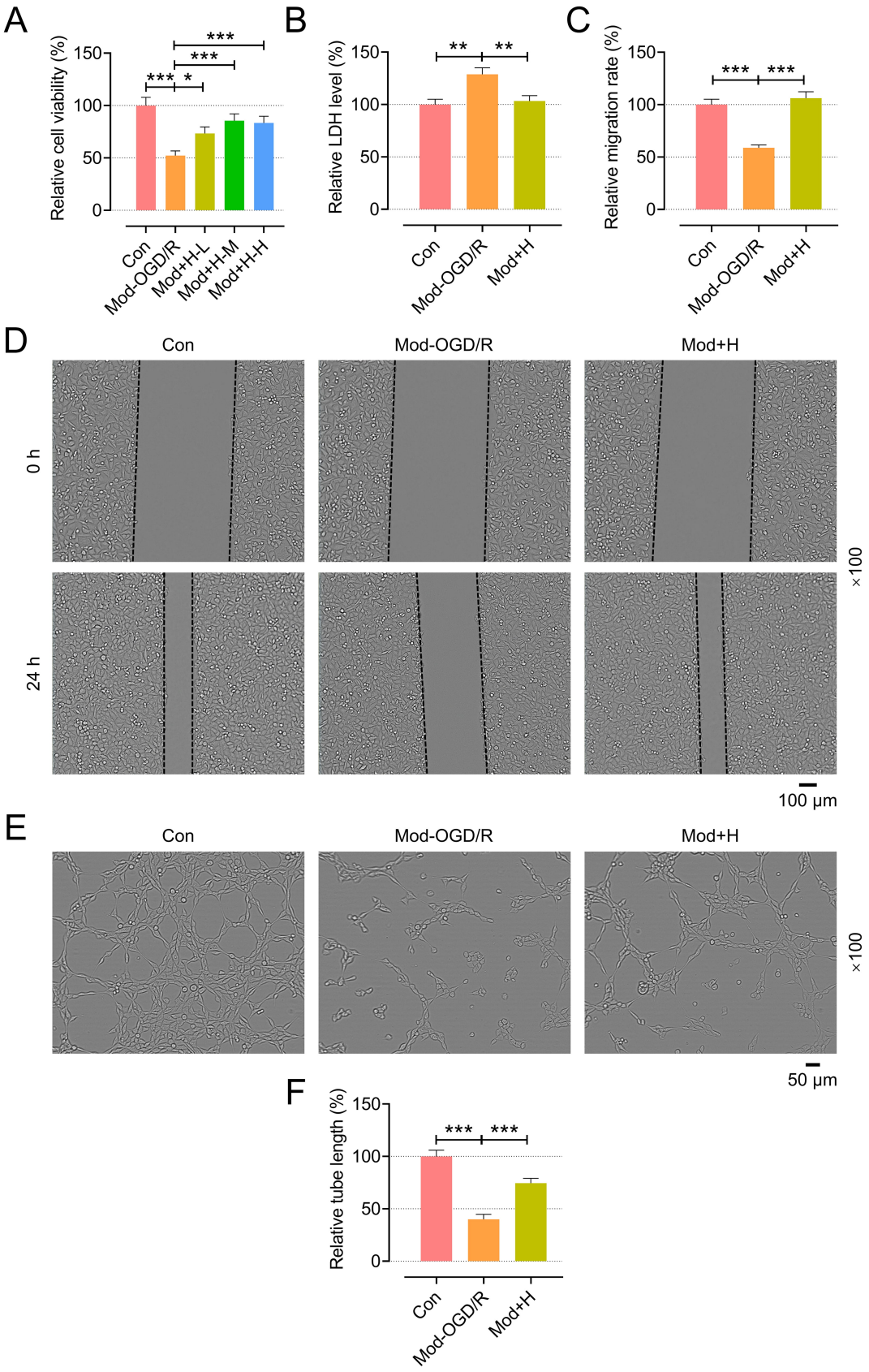

Fig. 4. Hirudin promotes cell vitality, migration, and angiogenesis, and downregulates lactate dehydrogenase (LDH). (A) Cell viability was measured by cell counting kit 8 (CCK-8). (B) Detection of LDH levels in cells. (C,D) Cell migration ability was detected by scratch test (scale bar: 100 μm, magnification; ×100). (E,F) The angiogenic ability of cells was measured by tube formation assay (scale bar: 50 μm, magnification; ×100). The experiment was repeated three times. *$p < 0.05$, **$p < 0.01$, ***$p < 0.001$.

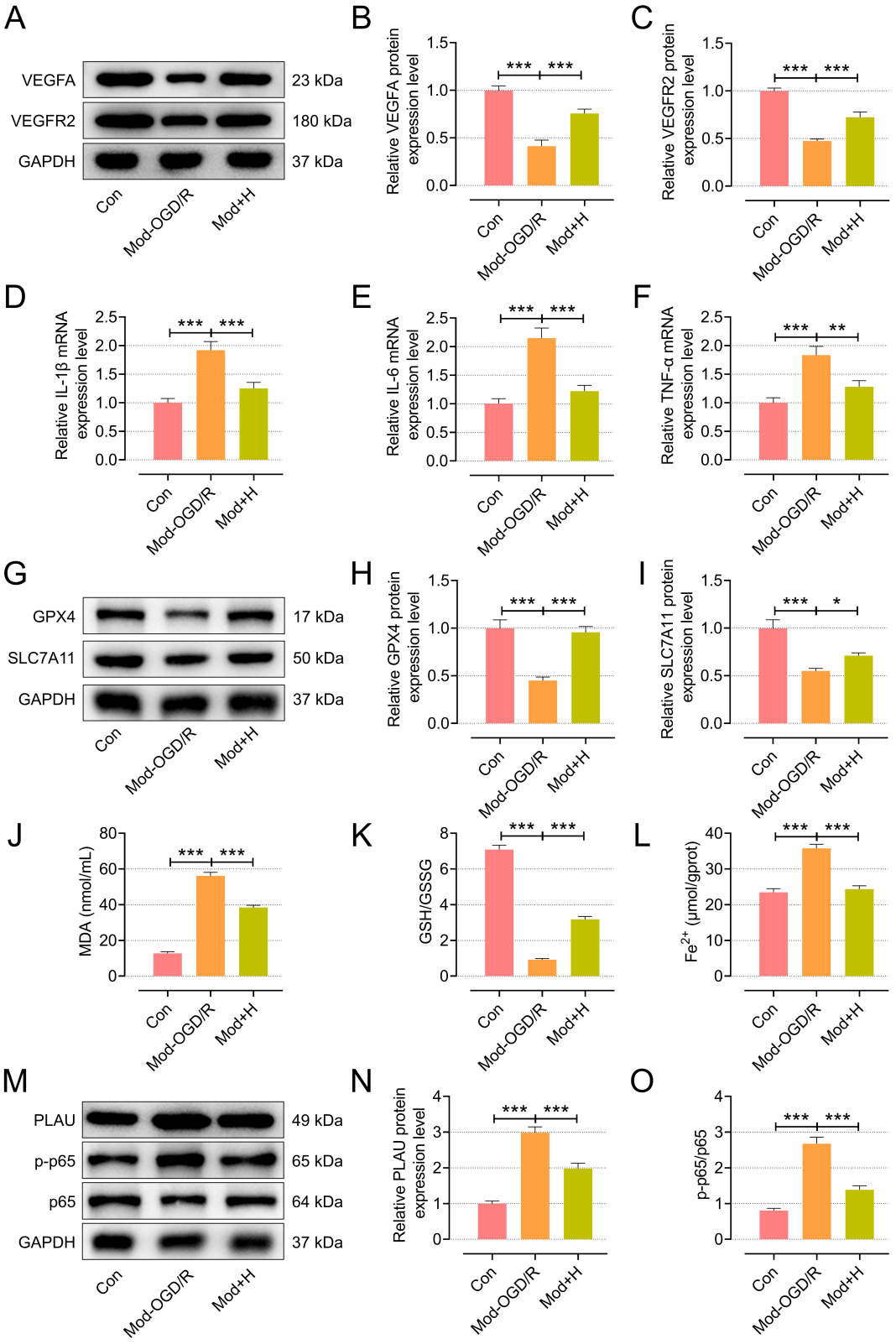

Fig. 5. Hirudin promotes angiogenesis and inhibits inflammation, ferroptosis, and PLAU/NF-κB. (A–C) The angiogenesis-related proteins VEGFA and VEGFR2 were detected by Western blotting. (D–F) The expression of inflammatory cytokines IL-1β, IL-6 and TNF-α was detected by qRT-PCR. (G–I) The expression of GPX4 and SLC7A11 in bEnd.3 cells was detected by Western blotting. GAPDH was the internal parameter. (J–L) The levels of MDA, GSH/GSSG and Fe^{2+} were detected by the kit. (M–O) The expression of PLAU/NF-κB in bEnd.3 cells was detected by Western blotting. GAPDH was used as the internal reference. The experiment was repeated three times. *$p < 0.05$, **$p < 0.01$, ***$p < 0.001$.

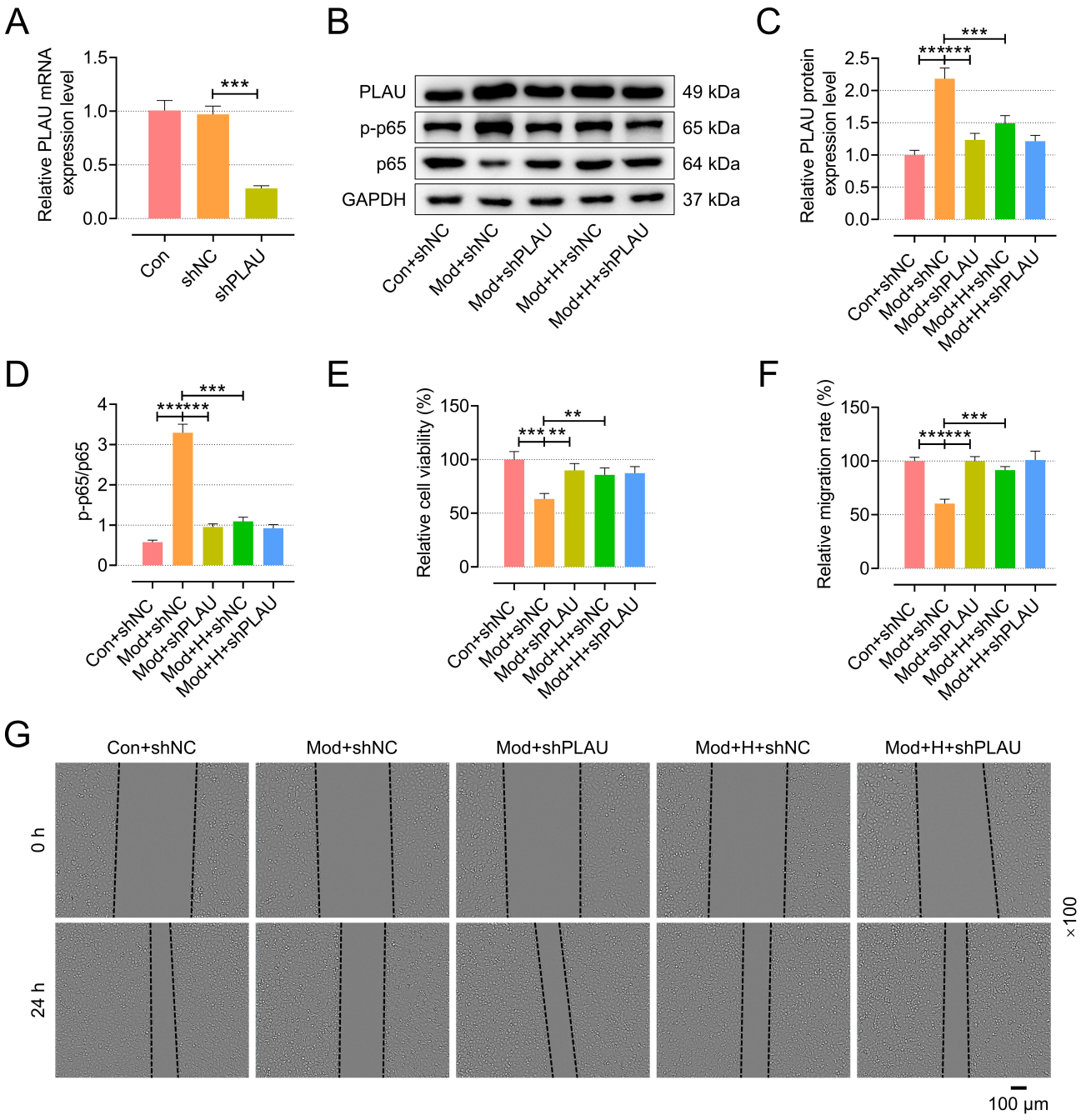

Fig. 6. Hirudin and silencing PLAU can both inhibit the activation of NF-κB and enhance cell viability and migration. (A) Transfection efficiency was measured by qRT-PCR. (B–D) PLAU, p-p65/p65 expression was detected by Western blotting. GAPDH was used as the internal reference. (E) Cell viability was measured by CCK-8. (F,G) Cell migration was detected by the cell scratch experiment (scale bar: 100 μm, magnification; ×100). The experiment was repeated three times. $^{**}p < 0.01$, $^{***}p < 0.001$.

< 0.01, Fig. 7I–N). These results indicate that hirudin can inhibit ferroptosis by down-regulating PLAU, thereby promoting endothelial vascular regeneration and improving ischemic stroke.

Discussion

The high morbidity, disability, and mortality associated with cerebral ischemia-reperfusion injury (CIRI) pose a serious threat to human health [29]. Hypoxia and nutritional deficiency kill neurons, which activate an inflammatory response and destroy the blood-brain barrier, causing irreparable brain tissue damage [30]. Notably, post-CIRI iron accumulation triggers ferroptosis, a process exacerbating tissue injury by promoting lipid peroxidation, while angiogenesis supports neural regeneration by supplying nutrients to the infarct area [31]. Thus, regulating both ferroptosis and angiogenesis is critical for CIRI treatment. This

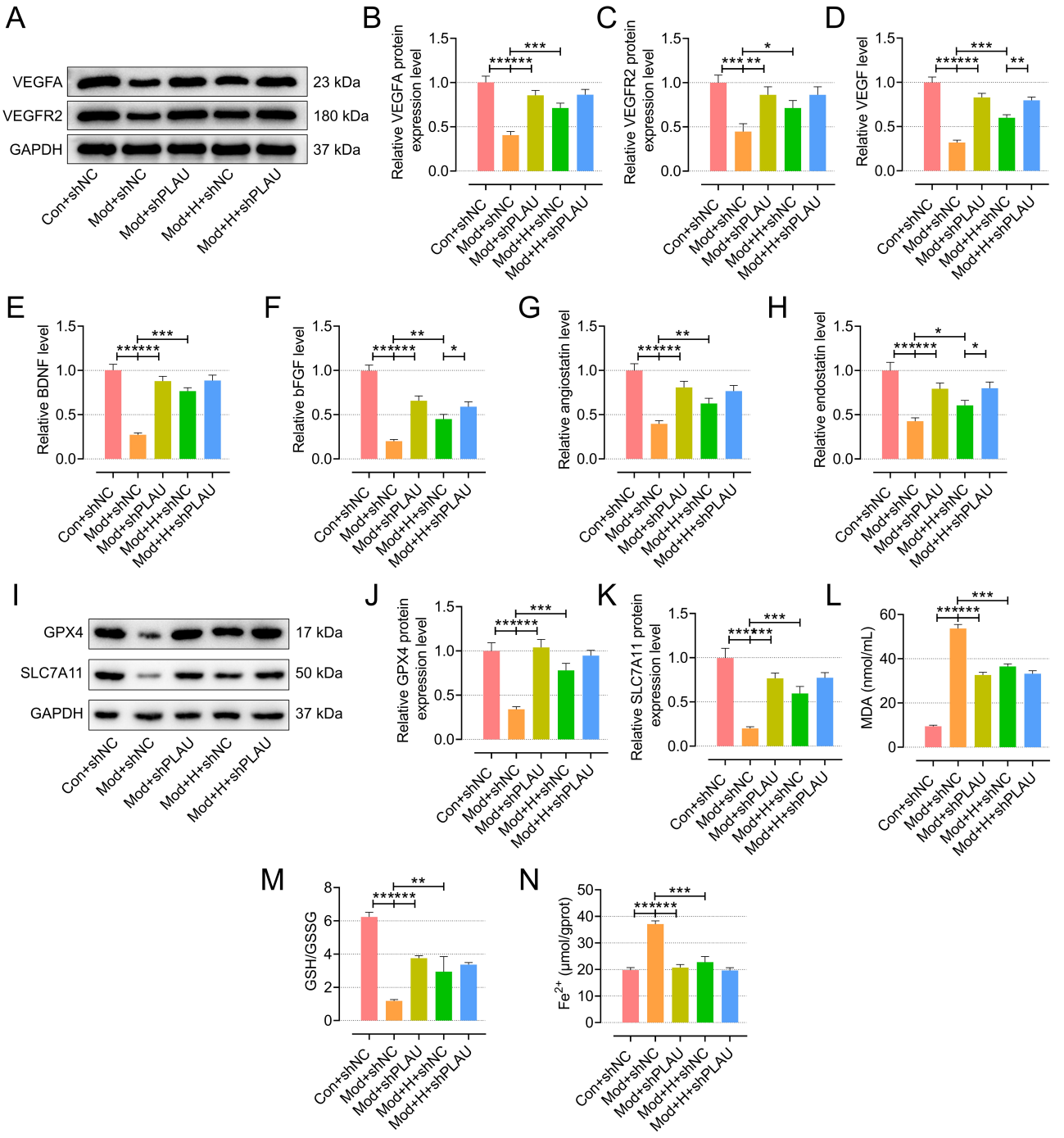

Fig. 7. Hirudin and PLAU silencing promote angiogenesis and attenuate ferroptosis. (A–C) Angiogenesis-related indexes VEGFA and VEGFR2 were detected by Western blotting. GAPDH was used as the internal reference. (D–H) ELISA was used to detect the secretion of angiogenesis-related factors, including VEGF, brain-derived neurotrophic factor (BDNF), basic fibroblast growth factor (bFGF), angiostatin and endostatin. (I–K) The expression of GPX4 and SLC7A11 in bEnd.3 cells was detected by Western blotting. GAPDH was used as the internal reference. (L–N) The levels of MDA, GSH/GSSG and Fe^{2+} were detected by the corresponding assay kit. The experiment was repeated three times. *$p < 0.05$, **$p < 0.01$, ***$p < 0.001$.

study focused on clarifying how hirudin alleviates CIRI by modulating the PLAU/NF-κB axis, ferroptosis, and angiogenesis.

PLAU, also known as urokinase plasminogen activator [32], encodes a serine protease, which, after binding to its receptor, promotes proteolysis and degradation of tumor cells' interstitial [33]. PLAU can also actively regulate biological processes such as cell migration, invasion and angiogenesis [34]. However, the role of PLAU in cerebral ischemia-reperfusion injury CIRI and its related mech-

anisms has been rarely elucidated. Research has found that PLAU can activate the NF-κB pathway [18]. Targeting PLAU can inhibit NF-κB activation to protect PC12 cells from damage caused by OGD/R treatment [19]. NF-κB is a key factor in the inflammatory signaling pathway, has the ability of multidirectional nuclear transcription, can regulate the expression of pro-inflammatory, pro-apoptotic and other genes, and participates in the pathogenesis of many diseases [35]. NF-κB inhibition is also associated with angiogenesis in cerebral ischemic injury [22,23].

Our study found that hirudin can down-regulate the expression of PLAU/NF-κB protein in the brain tissue of MCAO rats or in bEnd.3 cells after OGD/R treatment. The NF-κB protein p-p65/p65 was significantly down-regulated in bEnd.3 cells after PLAU silencing. Furthermore, hirudin increased GPX4/SLC7A11 (ferroptosis suppressors) and GSH/GSSG levels, while decreasing Fe^{2+} and MDA (ferroptosis markers), suggesting it inhibited ferroptosis via the inhibiting PLAU. Neuroinflammation is one of the major pathological responses associated with brain cell death in ischemic stroke [36]. During the acute phase, microglia in the brain are activated and release large amounts of inflammatory mediators, IL-1β, IL-6 and TNF-α, as well as the chemokine monocyte chemotactic protein 1 [36]. Our *in vivo* and *in vitro* studies have demonstrated that hirudin can down-regulate the inflammatory cytokines IL-1β, IL-6 and TNF-α in CIRI.

There are few reports on the treatment of CIRI with hirudin at present. Limited research has found that hirudin exerts neuroprotective effects by inhibiting CCL2-mediated ferroptosis and inflammatory pathways, or by activating the Wnt/β -catenin pathway to promote angiogenesis, thereby protecting against CIRI [37,38]. However, this study confirmed for the first time that hirudin may inhibit ferroptosis by down-regulating the expression of PLAU and suppressing the nuclear translocation of NF-κB/p65. It then promotes the transcription of downstream GPX4, thereby enhancing endothelial cell angiogenesis and improving ischemic stroke.

In order to further investigate the association between hirudin and brain injury angiogenesis, we also examined the expression of VEGFA and VEGFR2 in MCAO rats or bEnd.3 cells after OGD/R treatment. VEGF is an important growth factor with angiogenic activity, which can promote endothelial cell mitosis, anti-apoptosis, increase vascular permeability, and actively participate in the regulation of normal and pathological angiogenesis processes [39]. VEGFA, a member of the VEGF family, is the most effective and important vascular stimulating factor for angiogenesis and plays an important role in angiogenesis and pathological neovascularization [39,40]. VEGFR2 mediates the growth and survival signaling pathways of most endothelial cells, and is the main receptor responsible for VEGFA-induced mitosis, angiogenesis and permeability enhancement [39,41]. It was found that PLAU silence increased the expression of VEGFA/VEGFR2 in bEnd.3 cells after OGD/R treatment, which demonstrated that PLAU activation inhibited angiogenesis in brain injury, while hirudin treatment significantly increased the expression of VEGFA/VEGFR2 in CIRI. It is worth noting that in this study, the combined application of hirudin and PLAU gene silencing did not produce a more significant enhancement effect than single intervention in terms of cell viability, migration, and most angiogenesis indicators. This finding precisely supports our mechanistic inference, indicating that the core protective effect of hirudin is likely mediated by inhibiting the PLAU. When PLAU is effectively knocked down by shRNA, this pathway is fully inhibited, and the additional treatment with hirudin may not produce further pharmacological effects.

However, this study only focused on the PLAU/NF-κB axis, and the associations between other potential targets (such as CXCL12, MMP9) and angiogenesis have not been verified. Furthermore, only the short-term effects within 72 h after ischemia were observed. The influence of hirudin on the recovery of neurological function in the chronic phase and the potential bleeding risk need to be evaluated through long-term animal experiments.

Conclusion

In conclusion, hirudin alleviates CIRI by reducing infarct size and apoptosis, enhancing bEnd.3 cells viability, upregulating VEGFA/VEGFR2 to promote angiogenesis, inhibiting inflammation, and regulating ferroptosis-related indicators. These beneficial effects are associated with suppression of the PLAU/NF-κB axis. This study provides a reference for exploring the mechanism of vasogenesis of hirudin in CIRI and an experimental basis for its application in cardiovascular and cerebrovascular diseases.

Availability of Data and Materials

The analyzed datasets generated during the study are available from the corresponding author on reasonable request.

Author Contributions

MS, FS and WBL designed the research study. YFL, XDL and XWW performed the research. XYL, XSL and MLZ collected and analyzed the data. WBL has been involved in drafting the manuscript and all authors have been involved in revising it critically for important intellectual content. All authors gave final approval of the version to be published. All authors have participated sufficiently in the work to take public responsibility for appropriate portions of the content and agreed to be accountable for all aspects of the work in ensuring that questions related to its accuracy or integrity.

Ethics Approval and Consent to Participate

All procedures were approved by the Experimental Animal Welfare Ethics Committee of Zhejiang Experimental Animal Center (NO. ZJCLA-IACUC-20010713). All procedures complied with the ARRIVE Guidelines 2.0.

Acknowledgment

Not applicable.

Funding

This work was supported by the Zhejiang Rehabilitation Medical Center College level project (Grant No. ZKJC2503) and by Hangzhou Health Science and Technology Project (Grant No. B20252055).

Conflict of Interest

The authors declare no conflict of interest.

References

[1] Kalogeris T, Baines CP, Krenz M, Korthuis RJ. Ischemia/Reperfusion. Comprehensive Physiology. 2016; 7: 113–170. https://doi.org/10.1002/cphy.c160006.

[2] Ananth CV, Brandt JS, Keyes KM, Graham HL, Kostis JB, Kostis WJ. Epidemiology and trends in stroke mortality in the USA, 1975–2019. International Journal of Epidemiology. 2023; 52: 858–866. https://doi.org/10.1093/ije/dyac210.

[3] Qin C, Yang S, Chu YH, Zhang H, Pang XW, Chen L, *et al*. Signaling pathways involved in ischemic stroke: molecular mechanisms and therapeutic interventions. Signal Transduction and Targeted Therapy. 2022; 7: 215. https://doi.org/10.1038/s41392-022-01064-1.

[4] Lyden PD. Cerebroprotection for Acute Ischemic Stroke: Looking Ahead. Stroke. 2021; 52: 3033–3044. https://doi.org/10.1161/STROKEAHA.121.032241.

[5] Yang Y, Torbey MT. Angiogenesis and Blood-Brain Barrier Permeability in Vascular Remodeling after Stroke. Current Neuropharmacology. 2020; 18: 1250–1265. https://doi.org/10.2174/1570159X18666200720173316.

[6] Hatakeyama M, Ninomiya I, Kanazawa M. Angiogenesis and neuronal remodeling after ischemic stroke. Neural Regeneration Research. 2020; 15: 16–19. https://doi.org/10.4103/1673-5374.264442.

[7] Liu C, Wang G, Han W, Tian Q, Li M. Ferroptosis: a potential therapeutic target for stroke. Neural Regeneration Research. 2024; 19: 988–997. https://doi.org/10.4103/1673-5374.385284.

[8] Wang Y, Han J, Luo L, Kasim V, Wu S. Salidroside facilitates therapeutic angiogenesis in diabetic hindlimb ischemia by inhibiting ferroptosis. Biomedicine & Pharmacotherapy. 2023; 159: 114245. https://doi.org/10.1016/j.biopha.2023.114245.

[9] Zhang Y, Yang Y, Chen W, Mi C, Xu X, Shen Y, *et al*. BaP/BPDE suppressed endothelial cell angiogenesis to induce miscarriage by promoting MARCHF1/GPX4-mediated ferroptosis. Environment International. 2023; 180: 108237. https://doi.org/10.1016/j.envint.2023.108237.

[10] Li WQ, Qin ZS, Chen S, Cheng D, Yang SC, Choi YMM, *et al*. Hirudin alleviates acute ischemic stroke by inhibiting NLRP3 inflammasome-mediated neuroinflammation: In vivo and in vitro approaches. International Immunopharmacology. 2022; 110: 108967. https://doi.org/10.1016/j.intimp.2022.108967.

[11] Pang X, Zhang Y, Peng Z, Shi X, Han J, Xing Y. Hirudin reduces nephropathy microangiopathy in STZ-induced diabetes rats by inhibiting endothelial cell migration and angiogenesis. Life Sciences. 2020; 255: 117779. https://doi.org/10.1016/j.lfs.2020.117779.

[12] Yang X, Ou Y, Yang Y, Wang L, Zhang Y, Zhao F, *et al*. Targeting endothelial coagulation signaling ameliorates liver obstructive cholestasis and dysfunctional angiogenesis. Experimental Biology and Medicine. 2023; 248: 1242–1253. https://doi.org/10.1177/15353702231191190.

[13] Zhou HJ, Tang T, Cui HJ, Yang AL, Luo JK, Lin Y, *et al*. Thrombin-triggered angiogenesis in rat brains following experimental intracerebral hemorrhage. Journal of Neurosurgery. 2012; 117: 920–928. https://doi.org/10.3171/2012.8.JNS112152.

[14] Pan XY, Peng L, Han ZQ, Yin GQ, Song YK, Huang J. Hirudin promotes angiogenesis by modulating the cross-talk between p38 MAPK and ERK in rat ischemic skin flap tissue. Tissue & Cell. 2015; 47: 301–310. https://doi.org/10.1016/j.tice.2015.04.001.

[15] Liu J, Chen B, Zhao B, Luo X, Li J, Xie Y, *et al*. Effect of hirudin on arterialized venous flap survival in rabbits. Biomedicine & Pharmacotherapy. 2021; 142: 111981. https://doi.org/10.1016/j.biopha.2021.111981.

[16] De Paula EV, Nascimento MCF, Ramos CD, Ozelo MC, Machado TF, Guillaumon AT, *et al*. Early in vivo anticoagulation inhibits the angiogenic response following hindlimb ischemia in a rodent model. Thrombosis and Haemostasis. 2006; 96: 68–72. https://doi.org/10.1160/TH06-02-0103.

[17] Lin G, Lin B, Zhu J, Pan X, Yin G. Effect of natural hirudin on angiogenesis of human microvascular endothelial cells. Chinese Journal of Reparative and Reconstructive Surgery. 2018; 32: 1586–1591. https://doi.org/10.7507/1002-1892.201806055. (In Chinese)

[18] Meng T, Liu X, Zhang J, Li S, He W, Li W. MicroRNA-181b attenuates lipopolysaccharide-induced inflammatory responses in pulpitis via the PLAU/AKT/NF-κB axis. International Immunopharmacology. 2024; 127: 111451. https://doi.org/10.1016/j.intimp.2023.111451.

[19] Li N, Liu Y, Li JR, Zhang WX. Chrysin, which targets PLAU, protects PC12 cells from OGD/R-stimulated damage through repressing the NF-κB signaling pathway. Regenerative Therapy. 2022; 19: 69–76. https://doi.org/10.1016/j.reth.2021.11.002.

[20] Chen Y, Fang ZM, Yi X, Wei X, Jiang DS. The interaction between ferroptosis and inflammatory signaling pathways. Cell Death & Disease. 2023; 14: 205. https://doi.org/10.1038/s41419-023-05716-0.

[21] Mitchell JP, Carmody RJ. NF-κB and the Transcriptional Control of Inflammation. International Review of Cell and Molecular Biology. 2018; 335: 41–84. https://doi.org/10.1016/bs.ircmb.2017.07.007.

[22] Li Y, Liang W, Guo C, Chen X, Huang Y, Wang H, *et al*. Renshen Shouwu extract enhances neurogenesis and angiogenesis via inhibition of TLR4/NF-κB/NLRP3 signaling pathway following ischemic stroke in rats. Journal of Ethnopharmacology. 2020; 253: 112616. https://doi.org/10.1016/j.jep.2020.112616.

[23] Yingze Y, Zhihong J, Tong J, Yina L, Zhi Z, Xu Z, *et al*. NOX2-mediated reactive oxygen species are double-edged swords in focal cerebral ischemia in mice. Journal of Neuroinflammation. 2022; 19: 184. https://doi.org/10.1186/s12974-022-02551-6.

[24] Xia X, Li M, Wei R, Li J, Lei Y, Zhang M. Intracerebral hirudin injection alleviates cognitive impairment and oxidative stress and promotes hippocampal neurogenesis in rats subjected to cerebral ischemia. Neuropathology. 2023; 43: 362–372. https://doi.org/10.1111/neup.12897.

[25] Ren Y, Ma X, Wang T, Cheng B, Ren L, Dong Z, *et al*. The Cerebroprotein Hydrolysate-I Plays a Neuroprotective Effect on Cerebral Ischemic Stroke by Inhibiting MEK/ERK1/2 Signaling Pathway in Rats. Neuropsychiatric Disease and Treatment. 2021; 17: 2199–2208. https://doi.org/10.2147/NDT.S313807.

[26] Ku JM, Taher M, Chin KY, Grace M, McIntyre P, Miller AA. Characterisation of a mouse cerebral microvascular endothelial cell line (bEnd.3) after oxygen glucose deprivation and reoxygenation. Clinical and Experimental Pharmacology & Physiology. 2016; 43: 777–786. https://doi.org/10.1111/1440-1681.12587.

[27] Hou Y, Yang D, Zhang Q, Wang X, Yang J, Wu C. Pseudoginsenoside-F11 ameliorates ischemic neuron injury by regulating the polarization of neutrophils and macrophages in vitro. International Immunopharmacology. 2020; 85: 106564. https://doi.org/10.1016/j.intimp.2020.106564.

[28] Livak KJ, Schmittgen TD. Analysis of relative gene expression data using real-time quantitative PCR and the 2(-Delta Delta C(T)) Method. Methods. 2001; 25: 402–408. https://doi.org/10.1006/meth.2001.1262.

[29] Jurcau A, Simion A. Neuroinflammation in Cerebral Ischemia and Ischemia/Reperfusion Injuries: From Pathophysiology to Therapeutic Strategies. International Journal of Molecular Sciences. 2021; 23: 14. https://doi.org/10.3390/ijms23010014.

[30] Herpich F, Rincon F. Management of Acute Ischemic Stroke. Critical Care Medicine. 2020; 48: 1654–1663. https://doi.org/10.1097/CCM.0000000000004597.

[31] Ma R, Xie Q, Li H, Guo X, Wang J, Li Y, *et al*. *l*-Borneol Exerted the Neuroprotective Effect by Promoting Angiogenesis Coupled With Neurogenesis via Ang1-VEGF-BDNF Pathway. Frontiers in Pharmacology. 2021; 12: 641894. https://doi.org/10.3389/fphar.2021.641894.

[32] Vorstandlechner V, Laggner M, Copic D, Klas K, Direder M, Chen Y, *et al*. The serine proteases dipeptidyl-peptidase 4 and urokinase are key molecules in human and mouse scar formation. Nature Communications. 2021; 12: 6242. https://doi.org/10.1038/s41467-021-26495-2.

[33] Nantajit D, Chailapakul P, Bawornpatarapakorn S, Chamchod S, Laebua K. Prognostic significance of uPA and uPAR expression in patients with cervical cancer undergoing radiotherapy. Oncology Letters. 2021; 21: 423. https://doi.org/10.3892/ol.2021.12684.

[34] Gao Y, Ma X, Lu H, Xu P, Xu C. PLAU is associated with cell migration and invasion and is regulated by transcription factor YY1 in cervical cancer. Oncology Reports. 2023; 49: 25. https://doi.org/10.3892/or.2022.8462.

[35] Yu H, Lin L, Zhang Z, Zhang H, Hu H. Targeting NF-κB pathway for the therapy of diseases: mechanism and clinical study. Signal Transduction and Targeted Therapy. 2020; 5: 209. https://doi.org/10.1038/s41392-020-00312-6.

[36] Lambertsen KL, Finsen B, Clausen BH. Post-stroke inflammation-target or tool for therapy? Acta Neuropathologica. 2019; 137: 693–714. https://doi.org/10.1007/s00401-018-1930-z.

[37] Liao J, Chen H, Liao Y, Luo C, Wang Z, Zhang F, *et al*. Neuroprotective effects of hirudin against cerebral ischemia-reperfusion injury via inhibition of CCL2-mediated ferroptosis and inflammatory pathways. Brain Research Bulletin. 2025; 224: 111293. https://doi.org/10.1016/j.brainresbull.2025.111293.

[38] He L, Lei R, Li S, Zhao X, He X, Yang X, *et al*. Hirudin promotes cerebral angiogenesis and exerts neuroprotective effects in MCAO/R rats by activating the Wnt/β-catenin pathway. Journal of Stroke and Cerebrovascular Diseases. 2025; 34: 108218. https://doi.org/10.1016/j.jstrokecerebrovasdis.2024.108218.

[39] Apte RS, Chen DS, Ferrara N. VEGF in Signaling and Disease: Beyond Discovery and Development. Cell. 2019; 176: 1248–1264. https://doi.org/10.1016/j.cell.2019.01.021.

[40] White AL, Bix GJ. VEGFA Isoforms as Pro-Angiogenic Therapeutics for Cerebrovascular Diseases. Biomolecules. 2023; 13: 702. https://doi.org/10.3390/biom13040702.

[41] Patel SA, Nilsson MB, Le X, Cascone T, Jain RK, Heymach JV. Molecular Mechanisms and Future Implications of VEGF/VEGFR in Cancer Therapy. Clinical Cancer Research. 2023; 29: 30–39. https://doi.org/10.1158/1078-0432.CCR-22-1366.